Citation for published version:
Ciampa, F, Boccardi, S & Meo, M 2016, 'Factors affecting the imaging of the impact location with inverse filtering and diffuse wave fields', *Journal of Intelligent Material Systems and Structures*, vol. 27, no. 11, pp. 1523-1533. https://doi.org/10.1177/1045389X15596622

DOI:
10.1177/1045389X15596622

Publication date:
2016

Document Version
Peer reviewed version

Link to publication

University of Bath

Alternative formats
If you require this document in an alternative format, please contact:
openaccess@bath.ac.uk

General rights
Copyright and moral rights for the publications made accessible in the public portal are retained by the authors and/or other copyright owners and it is a condition of accessing publications that users recognise and abide by the legal requirements associated with these rights.

Take down policy
If you believe that this document breaches copyright please contact us providing details, and we will remove access to the work immediately and investigate your claim.

Download date: 04. May. 2023

Factors affecting the imaging of the impact location with inverse filtering and diffuse wave fields

Francesco Ciampa, Salvatore Boccardi, M. Meo*

Department of Mechanical Engineering, University of Bath, Bath BA2 7AY, UK

Abstract

Reciprocal time reversal (inverse filtering) of acousto/ultrasonic fields is a very efficient technique to focus elastic waves through reverberant isotropic and anisotropic media. Such a methodology relies on the correlation of the experimental Green's function that is acquired by a set of receiver sensors from a limited number of impact sources. However, although heterogeneities and discontinuities within the structural response can be compensated by the inverse filtering process, environmental effects such as temperature variations as well as incoherent noise measurements and the finite number of excitation sources may degrade the quality of time reversal focusing. The scope of this paper was to study the factors affecting the impact location imaging using the reciprocal time reversal method in the presence of complex diffuse wave fields. Particularly, a signal stretch strategy was developed to compensate the temperature changes before re-mitting the back propagated wave field at the focus point. Then, in order to investigate the imaging performance and the sensitivity of the proposed methodology, different set of libraries with reduced input signals were created and tested. Finally, different configurations of the receiver piezoelectric sensors were used to perform the reciprocal time reversal method. To validate this research work, two

* Corresponding author: m.meo@bath.ac.uk

geometrically complex composite structures, i.e. a composite tail rotor blade and a stiffened composite panel were employed. Results showed that both the temperature compensation and the signal processing with the reduced time traced signals and receiver sensors allowed obtaining an accurate identification of the impact events.

Keywords: impact localisation, composite structures, temperature compensation, inverse filtering, diffuse wave field.

I. Introduction

Composite materials are renowned for their high strength to weight ratio, resistance to fatigue and low thermal expansion. However, due to their fragility to low-velocity impacts, they present challenges for damage detection, as much of the flaw is often interlaminar (e.g. delamination, fibre breakage, etc…) and not readily detectable. Structural health monitoring (SHM) systems based on elastic guided wave (GW) diagnosis methods are one of the most advanced and mature techniques that can be used for the identification of the impact source (Ciampa and Meo, 2010a; De Marchi et al., 2011 and Ciampa and Meo, 2010b), as well as the impact force (Hu et al., 2007; Atobe et al. 2011; and Atobe et al., 2014). Although most of these techniques rely on the time of arrival (TOA) identification, the dispersive nature of GW and the presence of reverberant wave fields in geometrically complex structures can degrade the quality of its estimation, causing poor localisation. However, reciprocal time reversal (TR) or inverse filtering (IF) method has shown to compensate the dispersive behaviour of GW, even in dissipative media with diffuse wave field conditions (i.e. with random scattering, reflection from the boundaries, mode conversion, etc…) (Ciampa and Meo,

2012a). In addition, reciprocal TR has been recently used for a chaotic cavity transducer implementation (Van Damme et al., 2011) and in nonlinear elastic imaging (Ciampa and Meo, 2012b). Indeed, IF approach uses the benefits of diffuse elastic waves that are generated by an impulsive excitation, in order to obtain the re-focusing at the impact source with a relative low number of receivers transducers. Particularly, according to the hypothesis of time invariance and spatial reciprocity of the linear wave equation, in the IF process the output received by a set of receiver sensors can be time reversed, normalised by its squared modal energy and re-emitted back onto the excitation point (Tanter et al., 1998). As GW have a number of wave packets whose speed depends on the propagation frequency, after the IF process the slower modes are back propagated first, so that all the waveforms will converge at the original impact point at the same time, thus compensating dispersion (Ciampa and Meo, 2011). However, environmental changes can negatively influence the library of the measured GW signals (Weaver and Lobkis, 2000). Among various environmental conditions, temperature variations are one of the most dominant effects that may alter the acquired waveforms, leading to ambiguities in the temporal and spatial re-focusing at the impact source (L di Scalea and Salamone, 2008). Hence, strategies for overcoming this further limitation due to temperature changes need to be developed. In particular, optimal baseline selection (Lu Y, Michaels, 2005) and the optimal signal stretch (Caputi, 1971) were implemented on a baseline subtraction technique (Worden et al., 2007). Ribay et al (2007) developed a temperature compensation technique for time reversal process in simple plate-like structure. In particular, they showed that temperature variations in aluminium and glass plates from 25ºC to around 50ºC dramatically decreased the values of the TR correlation coefficients at the impact location up to 30%. However, a systematic and effective

analysis of those environmental effects that might negatively influence the IF imaging at the impact location in “real” aerospace structures, especially at low temperatures, is still needed.

The scope of this paper was to study the factors affecting the re-focusing at the impact location using the reciprocal TR method in the presence of complex diffuse wave fields. Firstly, a signal stretch procedure was developed in order to compensate the temperature variations before performing the IF process. Then, in order to improve the imaging performance and thus decreasing the computational demand but not the sensitivity of the proposed methodology, different set of libraries with reduced input signals were created and analysed. Finally, different configurations of the receiver piezoelectric sensors were used to perform the reciprocal TR method in the presence of incoherent measurement noise due to electronics (sensor noise, electronic noise, etc…). To validate this work, two complex composite structures, i.e. a composite tail rotor blade and a stiffened composite panel were employed. The imaging results showed that the temperature compensation method and the signal processing with the reduced impulsive waveforms and receiver sensors allowed achieving an accurate re-focusing at the impact source, regardless the sensors type and position. The layout of the paper is as follow: in Section II, the effects of temperature variations on the diffuse wave fields are reported and a novel temperature compensation technique, called “forward step signal stretch” (FSSS) is introduced. Section III describes the experimental set-up for two different composite structures, whilst Section IV illustrates the IF imaging results of the impact source using the temperature compensation method with a reduced number of input signals and receivers sensors. Then, the conclusions of this research work are presented.

II. Theoretical Aspects of Inverse Filtering with Diffuse Wave Fields

If the time reversal invariance and the spatial reciprocity of the elastodynamic wave equation are satisfied, the reciprocal TR or IF process can be used to focus ultrasonic waves in reverberant anisotropic media (Ulrich et al., 2009). According to Huygen's principle (Landau and Lifshitz, 1960), the reconstruction of the wave function in a generic volume can be obtained by the knowledge of its sources located on a 2D surface. IF method is usually split into two steps. In the "forward propagation step", a set of signals representing a library of impulse responses from M excitation points at locations $\mathbf{r}_m$ (with $\mathbf{r}_m = x_1\hat{i} + x_2\hat{j} + x_3\hat{k}$ in Lagrangian coordinates x_j) along the plane of the structure (known as "focusing plane") is recorded by a number of surface bonded receiver transducers and stored. The wave field $\psi(\mathbf{r},t)$ measured in $\mathbf{r}$ at time t by an impulsive force located in $\mathbf{r}_m$ can be expressed as:

$$\psi(\mathbf{r},t) = \sum_{m=1}^{M} G(\mathbf{r},t;\mathbf{r}_m) \underset{t}{\otimes} e(\mathbf{r}_m,t) \tag{1}$$

where $G(\mathbf{r},t;\mathbf{r}_m,t_0)$ correspond to the Green space-time function that describes the linear propagation from the mth excitation point $(1 \le m \le M)$ to the receiver sensor and $e(\mathbf{r}_m,t)$ is the impulsive point-like source (Ciampa and Meo, 2014). Assuming a non-stationary Gaussian signal with zero mean and a variance $\sigma^2(t)$ that changes with time, the Green's function for a reverberant medium with diffuse field conditions becomes (Larose et al., 2006; Weaver, 1982 and Lobkis and Weaver, 2001):

$$G(\mathbf{r},t;\mathbf{r}_m) = \sum_{m=1}^{M}\sum_{n=1}^{N} a_m^n(t)\psi_m^n(\mathbf{r})\exp\left[-i\omega^n\left(t-t^n\right)\right] \tag{2}$$

where $a_m^n(t)$ are complex modal amplitudes and $\psi_m^n(\mathbf{r})$ are the real orthogonal mode shapes. Time t^n represents the travel time corresponding to the nth $(1 \le n \le N)$ scattering path within the sample. The second step, known as "backward propagation step", consists of a correlation between the impulsive transfer function associated to each excitation point and the inversion of the structural response of a new impact of unknown position $\mathbf{r}_{m0}$. In this manner, by using the benefits of a reverberant diffuse wave field (i.e. multiple scattering, reflections form the boundaries, mode conversion, etc…), the information on the impact source location is accomplished by the imaging process as the maximum of the IF correlation coefficients at the focus point (i.e. when $\mathbf{r}_m = \mathbf{r}_{m0}$). This can be expressed in the time domain as the correlation of diffuse fields (CDF) as follows:

$$e_{IF}(\mathbf{r}_m, t) = \frac{1}{\left\| G(\mathbf{r}, t; \mathbf{r}_m) \right\|} G(\mathbf{r}_m, t; \mathbf{r}) \underset{t}{\otimes} G(\mathbf{r}, -t; \mathbf{r}_{m0}) \qquad (3)$$

Moreover, in order to compensate the incoherent measurement noise due to electronics, a weighted average from the contribution of a number of L surface bonded receiver sensors was used (Ciampa and Meo, 2014). As the quality of the library of signals acquired in the "forward propagation step", as well as the number of the M excitation points and the receiver transducers control the sensitivity of the imaging process, some forms of compensation techniques are required.

II.1 Effects of Temperature Variations on Diffuse Wave Fields

Assuming the excitation function as a Dirac delta function in time and space, $e(\mathbf{r}_m, t) = \delta(\mathbf{r}_m, t)$, the diffuse wave field originated from each mth excitation point on the

focusing plane at the reference temperature T_0 can be expressed substituting Eq. (2) in (1) as follows (Ing et al., 2005):

$$\psi(\mathbf{r},t;T_0) \cong G(\mathbf{r},t;\mathbf{r}_m) \tag{4}$$

If there is a change of temperature $\Delta T = T_* - T_0$, with $T_* \neq T_0$, each of the individual modes is altered in the travel time so that the new propagating wave field $\psi(\mathbf{r},t;T_*)$ is a time-delayed version of the reference wave field $\psi(\mathbf{r},t;T_0)$. Indeed, the effect of homogeneous temperature variations on the elastic wave propagation consists of a change of the wave speed that results either to a time dilation or compression of the travel time t^n (Snieder et al., 2002). Hence, according to Eqs. (2) and (4), the new time-shifted signal at temperature T_* can be defined as:

$$\psi(\mathbf{r},t;T_*) = \sum_{m=1}^{M}\sum_{n=1}^{N} a_m^n(t)\psi_m^n(\mathbf{r})\exp\left[-i\omega^n\left(t-\gamma t^n\right)\right] \tag{5}$$

where the (constant) coefficient γ is introduced as a perturbation of the wave field due to temperature changes (Leroy and Derode, 2008). In other words, the structural impulsive response from each excitation point under diffuse wave field conditions can be expressed as $\sum_{n=1}^{N} a_m^n(t)\psi_m^n(\mathbf{r})\exp\left[-i\omega_m^n\left(t-q^n\right)\right]$ along the N multiple scattering trajectories with a signal received with a time delay $q^n = \gamma t^n$. Fig. 1 represents the normalised time-shifted impulsive responses measured at two different temperatures (from the same excitation point) by four different receivers surface bonded on the sandwich composite panel defined in Sec. III. In particular, the dashed blue ones correspond to the signals acquired at the reference temperature T_0 = 21ºC, whilst the continuous black waveforms are taken at T_* = 5ºC.

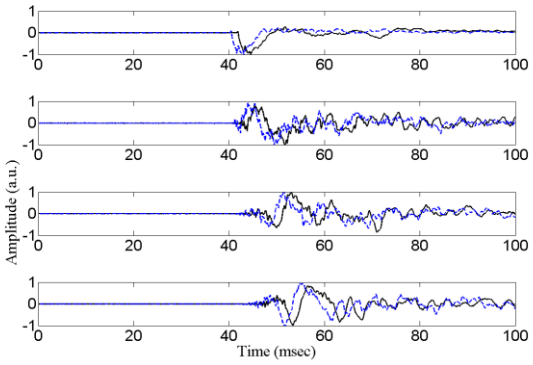

Figure 1 Normalised time histories measured by four receiver sensors on the sandwich composite panel at two different temperatures. The dashed blue signals are measured at T_0 = 21°C, whilst the black continuous ones are at T_* = 5°C.

Hence, in order to compensate the temperature effects, a signal stretch strategy called forward step signal stretch (FSSS) is applied to the library of impulsive transfer functions acquired in the "forward propagation step" of the IF process.

II.2 Forward Step Signal Stretch

As seen in Section II.1, temperatures changes affect the speed of the elastic waves causing either dilation or compression of the travel times of the scattered wave fields. Forward step signal stretch (FSSS) is herein introduces as a fast and efficient temperature compensation technique able to improve the image contrast at the impact source (Ciampa and Meo, 2011 and Catheline et al., 2007). Indeed, FSSS is a simple iterative process in which the diffuse wave field $\psi(\mathbf{r},t;T_0)$ originated from the focus point $\mathbf{r}_{m0}$ in the "forward propagation step" is stretched (where the term stretched refers to both dilation and compression) by a stretch factor $\tilde{\gamma}$ (unknown) to obtain a new impulsive structural response $\tilde{\psi}(\mathbf{r},t;T_0,\tilde{\gamma})$ that matches the one obtained at temperature T_*. This last term can be expressed as:

$$\tilde{\psi}(\mathbf{r},t;T_0,\tilde{\gamma}) = \psi(\mathbf{r},t/\tilde{\gamma};T_0) = \sum_{m=1}^{M}\sum_{n=1}^{N} a_m^n(t)\psi_m^n(\mathbf{r})\exp\left[-i\omega_m^n\left(t/\tilde{\gamma}-t^n\right)\right] \quad (6)$$

The stretch factor $\tilde{\gamma}$ is then applied to all the signals of the library from each of the M excitation points. The iterative algorithm to retrieve the value of $\tilde{\gamma}$ is implemented as follows.

Initially, the IF experiment is performed at temperature T_* different from the reference one and $e_{IF}(\mathbf{r}_m,t)$ is calculated according to Eq. (4). The obtained 2D image, due to temperature variations effects, will contain artefacts and ambiguities that need to be compensated for a correct visualisation of the impact source. Then, the diffuse wave field $\psi(\mathbf{r},t;T_0)$ originated from $\mathbf{r}_{m0}$ [i.e. that corresponding to the maximum value of $e_{IF}(\mathbf{r}_m,t)$] with a fixed acquisition time τ is stretched in both time and frequency domains. For a given sampling time Δt, the discretely sampled signal is $\psi_1[\mathbf{r},k;T_0]=\psi(\mathbf{r},k\Delta t;T_0)$ where k is an integer that corresponds to the sample at time $k\Delta t$ containing a total of p points. In our experiments, $\Delta t = 10.05\,\mu s$ and p = 9956 samples. In order to perform the time-stretch, $\psi_1[\mathbf{r},k;T_0]$ is first padded with zeroes so that it now contains a total of p_1 points sampled with a sampling time equal to Δt_1. The number of points p_1 is arbitrarily decided and it is maintained fixed for all the iterations. The obtained discretely diffuse wave field is then transformed in the frequency domain using a Fast Fourier transformation (FFT) operation. The resulting signal is a discretely sampled spectrum $\hat{\psi}_1[\mathbf{r},k;T_0]$ containing p_1 points (the symbol "$\hat{\cdot}$" corresponds to a FFT operation), with a frequency spacing between points equal to $\Delta f_1 = 1/p_1\Delta t_1$. The spectrum is then either truncated or zero-padded to create a new spectrum $\hat{\psi}_2[\mathbf{r},k;T_0]$ that contains p_2 points. The truncation or padding takes place in a way that it preserves

the conjugate symmetry of the whole spectrum according to the implementation of the FFT algorithm. The modified spectrum is then subjected to an inverse FFT, resulting in a new discretely sampled representation of the original wave field $\psi_2[\mathbf{r},k;T_0]=\psi(\mathbf{r},k\Delta t_2;T_0)$, containing p_2 points sampled with a sampling time $\Delta t_2 = 1/p_2\Delta f_1 = (p_1/p_2)\Delta t_1$. It should be noted that this operation has not yet performed the time-stretch of the original waveform, but it has simply re-sampled $\psi_1(\mathbf{r},t;T_0)$ with a different time step Δt_2. However, if a new continuous signal is defined as $\psi_2(\mathbf{r},t;T_0)=\psi(\mathbf{r}_m,t/\tilde{\gamma};T_0)$ where $\tilde{\gamma}=p_2/p_1$, then it can be seen that $\psi_2[\mathbf{r},k;T_0]$ is the discrete representation of $\psi_2(\mathbf{r},t;T_0)$ sampled with the original time step Δt_1. During the iteration, the factor $\tilde{\gamma}$, and so the number of points p_2, is varied in order to find the value that matches the wave field at different temperatures. Particularly, the stretch factor $\tilde{\gamma}$ is obtained as the minimum value between the maximum residual of the signal $\psi(\mathbf{r},t/\tilde{\gamma};T_0)$ calculated at the impact location in the "forward propagation step" and the new impact source $\psi(\mathbf{r},t;T_*)$ acquired in the "backward propagation step". According to Eq. (5), this can be expressed as:

$$\tilde{\gamma}=\arg\min_{\tilde{\gamma}}\left\{\max\left\|\psi(\mathbf{r},t;T_*)-\tilde{\psi}(\mathbf{r},t;T_0,\tilde{\gamma})\right\|\right\} \tag{7}$$

It should be noted that as $\Delta t \neq \Delta t_1$, the signal sampled in the "forward propagation step" and that obtained in the "backward propagation step" have different lengths. In order to have arrays of the same dimension p, the stretched signals are simply truncated. Once the value of $\tilde{\gamma}$ is determined by the FSSS algorithm, it is applied to the M excitation signals on the "focusing plane" so that a new IF process can be performed and new image of the impact source at the focus point can be obtained. Fig. 2 shows the original

waveform (dashed blue signal) acquired at T_0 and the new one (continuous black signal) measured at T_* and stretched after FSSS process. Similarly to Fig. 1, the impulse was applied on the same excitation point and it was recorded using four receiver sensors attached on the composite stiffened panel.

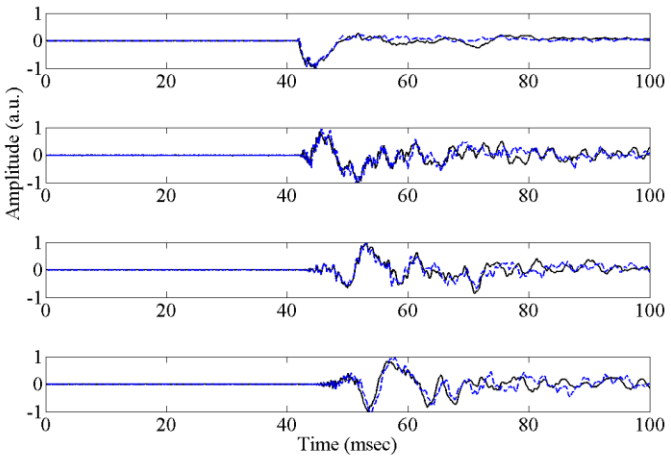

Figure 2 Normalised time histories measured by four receiver sensors on the sandwich composite panel before and after the FSSS process. The dashed blue signals are the original signals measured at T_0, whilst the black continuous ones are obtained after FSSS.

III. Experimental Set-up

A number of experiments were investigated on two composite structures. The first sample tested was a composite tail rotor blade of a helicopter with dimensions 125 x 20 x 2 cm (Fig. 3).

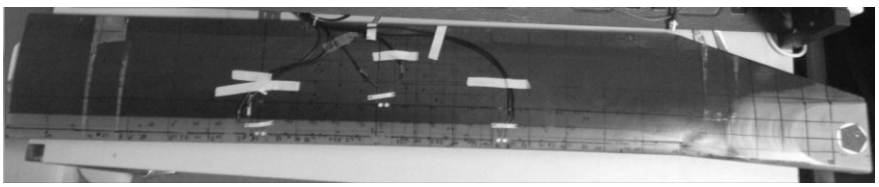

Figure 3 Tail rotor blade used during the experiments.

Although no quantitative information was provided on the mechanical properties and the structural make-up, the leading edge of the blade was made of glass fibre reinforced plastic (GFRP) for impact damage tolerance, whilst carbon fibre reinforced plastic (CFRP) was used for the rest of the blade to increase the structural strength and stiffness. The passive sensors used were $L = 4$ surface bonded piezoelectric transducers (APC sensors) with diameter of 0.635 cm, thickness of 0.25 cm and central frequency of 100 kHz. Sensors positions are reported in Table 1. The reference systems was arbitrarily chosen, with the origin at the bottom left corner of the structure and the x and y-axes parallel and perpendicular to the leading edge direction, respectively.

	X (cm)	**Y (cm)**
Sensor 1	37.7	1.5
Sensor 2	38.7	1.5
Sensor 3	75.2	1.5
Sensor 4	76.2	1.5

Table 1. Sensors positions on the tail rotor blade

The structural surface of the blade was divided in $M = 17 \times 6$ excitation points. The size of the single cell was not constant, but varied from smaller cells of dimensions 3 x 2 cm on the GFRP region, to bigger cells of dimensions 3 x 3 cm on the CFRP region. Such a configuration was designed to improve the resolution at the leading edge of the blade, as that is the area mostly subjected to impacts. The second structure was a rectangular CFRP composite stiffened panel with dimensions 100 x 30 x 0.2 cm. The "focusing plane" was divided in M = 50 x 15 excitation points uniformly distributed along a grid of quadratic cells with dimensions of 2 cm (Fig. 4).

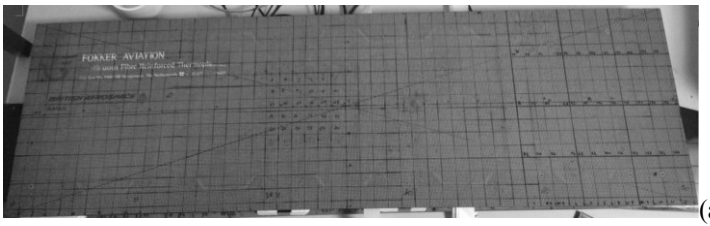

(a)

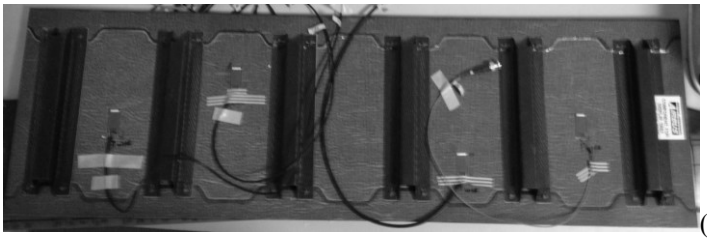
(b)

Figure 4 Front (a) and back (b) views of the composite stiffened panel.

As for the blade, the manufacturer did not provide any information regarding to the structural properties. The panel was reinforced by six stiffeners (25 x 7 x 2.5 cm) of hollow square cross-section attached to the structure through four rivets. The passive sensors mounted on this sample were $L = 4$ Macro-Fibre Composite transducers (MFC) with length 27.2, width 13.8 and thickness 0.3 mm. Sensors were glued on the back of the panel as shown in Fig. 4b and positioned at coordinates reported in Table 2, whilst the impacts were applied on the top surface. Due to the small thickness of the skin, clear impact responses were measured by the receiver transducers. The origin of the new reference frame was at the bottom left corner and the x and y-axes were oriented parallel to the edges of the panel.

	X (cm)	Y (cm)
Sensor 1	83.7	15.2
Sensor 2	65.7	21
Sensor 3	31	8.5
Sensor 4	13.5	15.2

Table 2. Sensors positions on the composite stiffened panel

Both structures were impacted manually with an uncontrolled system (modal hammer) and the waveforms were recorded using the NI PXI-5105 8-channel digitizer/oscilloscope card. The waveforms acquired in each cell of the "focusing plane"

in the “forward propagation step” were averaged 15 times to eliminate any random noise. Each impulsive response was sampled at 99.5 kHz with a total acquisition time of 100 ms according to Nyquist theorem and the long reverberation present in the recorded waveforms (Fig. 5).

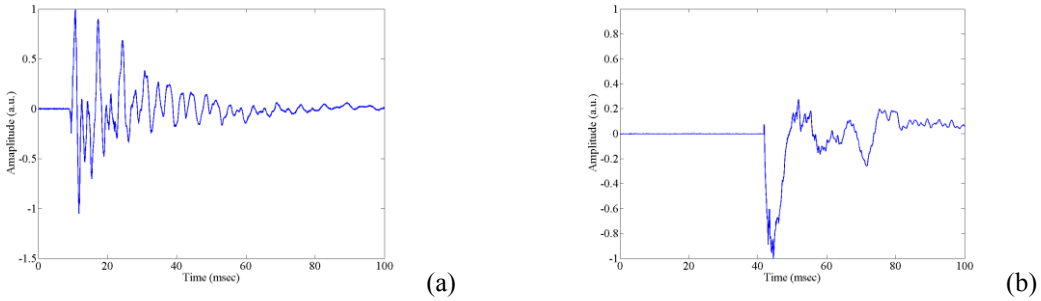

Figure 5 Normalised time history from one of the excitation points measured on the tail rotor blade (a) and the stiffened panel (b).

For the temperature compensation experiments, both structures were placed in a controlled room capable of reaching -3ºC. The temperature of the samples was monitored by two K-type thermocouples connected to a thermometer with a precision of 0.1ºC.

IV. Imaging Localisation Results

This Section illustrates the imaging results with the FSSS method used to compensate the wave speed changes of diffuse wave fields due to temperature variations. Then, in order to decrease the computational demand of the stored data but not the sensitivity of the proposed methodology, different set of libraries with reduced excitation points were created and tested. Finally, different configurations of the receiver piezoelectric sensors were used to perform the reciprocal TR technique .

IV.1 Imaging Results with the Temperature Compensation Method

Among the numerous successful tests performed with FSSS and reciprocal TR, two experiments for both structures introduced in Section III are reported in this paper for two different impact positions at different temperatures. In particular, Tables 3 and 4 report the impact coordinates and the temperature variations between the reference temperature T_0 and the current one T_* for the composite blade and the sandwich panel, respectively.

	X (cm)	Y (cm)	T_0 (ºC)	T_* (ºC)
Impact B1	25	4	21	0
Impact B2	72	10	21	5

Table 3. Impact positions for the and corresponding temperatures for the composite tail rotor blade

	X (cm)	Y (cm)	T_0 (ºC)	T_* (ºC)
Impact S1	6	3	21	0
Impact S2	80	10	21	5

Table 4. Impact positions for the and corresponding temperatures for the composite stiffened panel

According to Section II.2, the stretch factor $\tilde{\gamma}$ is first calculated by means of FSSS and then, the refocusing wave field at the impact location is represented as the maximum of a normalised 2D map given by Eq. (3). The impact source is deduced from the highest value (nearest to one) of the IF correlation coefficients as a weighted average from the contribution of four surface bonded receiver sensors. Fig. 6 reports the 2D imaging results of the impact location on the composite blade for impacts B1 (a, b, c) and B2 (d, e, f).

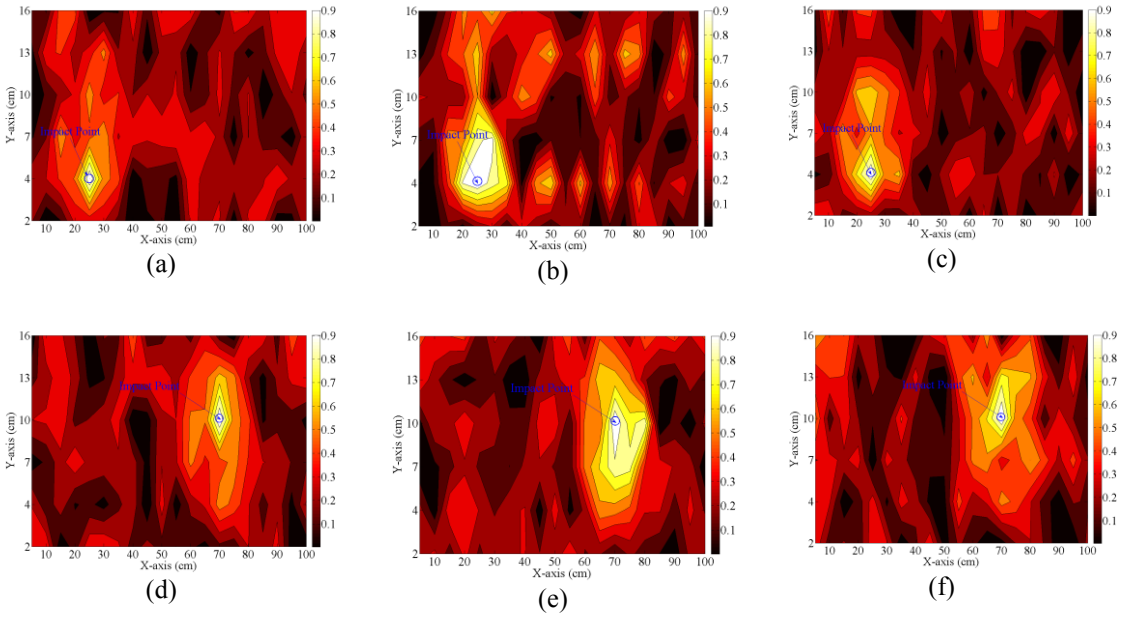

Figure 6 2D imaging results of the impact location for impacts B1 (a, b, c) and B2 (d, e, f). In (a) and (d) the signals in the "forward propagation step" and "backward propagation step" are measured at the same temperature T_0. In (b) and (e) the signals measured in the "backward propagation step" are taken at $T_* \neq T_0$, whilst (c) and (f) show the 2D maps after FSSS.

Figs. 6(a) and (d) depict the image of the impact location obtained with the wave fields measured at the reference temperature T_0 both in the "forward propagation step" and "backward propagation step". Figs. 6(b) and (e) illustrate the 2D maps with the signal acquired in the "backward propagation step" at a temperature different from the reference one, i.e. at T_* = 0ºC and T_* = 5ºC, respectively. Figs. 6(c) and (f) show the results of the imaging method after the FSSS process. Similar results were obtained in Fig. 7 with the stiffened panels for impact S1 (a, b, c) and S2 (d, e, f).

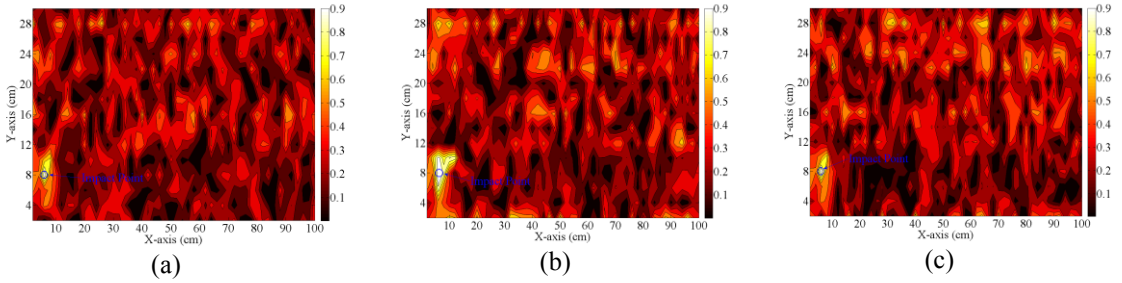

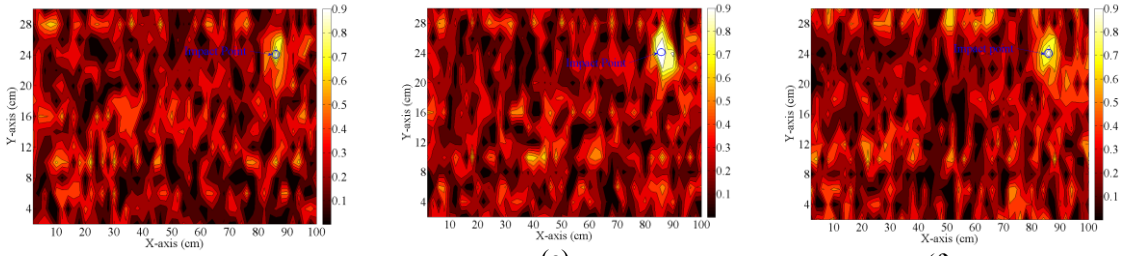

Figure 7 2D imaging results of the impact location for impacts S1 (a, b, c) and S2 (d, e, f). In (a) and (d) the signals in the "forward propagation step" and "backward propagation step" are measured at the same temperature T_0. In (b) and (e) the signals measured in the "backward propagation step" are taken at $T_* \neq T_0$, whilst (c) and (f) show the 2D maps after FSSS.

From the above figures, it can be clearly seen that due to temperature variations, the normalised correlation coefficients are still maxima (or close to one) at the focus point but also in locations adjacent to the impact source [Figs. 6, 7(b) and (e)]. This inevitably creates ambiguities in retrieving the impact location that can be eliminated using the FSSS process. Indeed, the temperature variations effects were mitigated due to a higher contrast between the maximum IF correlation coefficient at position $\mathbf{r}_{m0}$ and in other locations on the focusing plane [Figs. 6, 7(c) and (f)]. Finally, it should be noted that, theoretically, padding the discretely sampled with zeroes in the time-axis would introduce some frequency distortions (Clarke et al., 2008). However, within the frequency range of the recorded diffuse fields, those effects were marginal and did not affect the re-focusing at the impact source.

IV.2 Imaging Results with Reduced Excitation Points

In all the experiments shown in Figs. 6 and 7, the number of excitation points on the focusing plane was M = 17 x 6 for the tail rotor blade and M = 50 x 15 for the stiffened panel. In this Section, a different set of libraries with a reduced number of excitation points was created and tested in order to improve the imaging performance and thus to

decrease the computational demand of the stored waveforms. Once more, according to Eq. (3), the 2D maps were generated as a weighted average from the contribution of L = 4 receiver sensors and, for simplicity, without undermining validity of the results, all the signals measured were taken at the same reference temperature T_0 = 21ºC. Among all tests performed, two different experiments are reported in Figs. 8 and 9 for both the composite blade (namely Br1 and Br2) and the stiffened panel (namely Sr1 and Sr2) with two different set of reduced excitation points. Tables 5 and 6 provide information about the real and detected impact coordinates, as well as the numbers of excitations points M.

	Br1	**Br2**
X (cm) (real value)	6	80
X (cm) (detected value)	9	80
Y (cm) (real value)	3	7
Y (cm) (detected value)	2	10
M	13 x 5	10 x 4

Table 5. True and detected impact positions corresponding to different excitation points on the tail rotor blade

	Sr1	**Sr2**
X (cm) (real value)	52	42
X (cm) (detected value)	52	44
Y (cm) (real value)	12	18
Y (cm) (detected value)	10	20
M	40 x 12	37 x 11

Table 6. True and detected impact positions corresponding to different excitation points on the stiffened panel

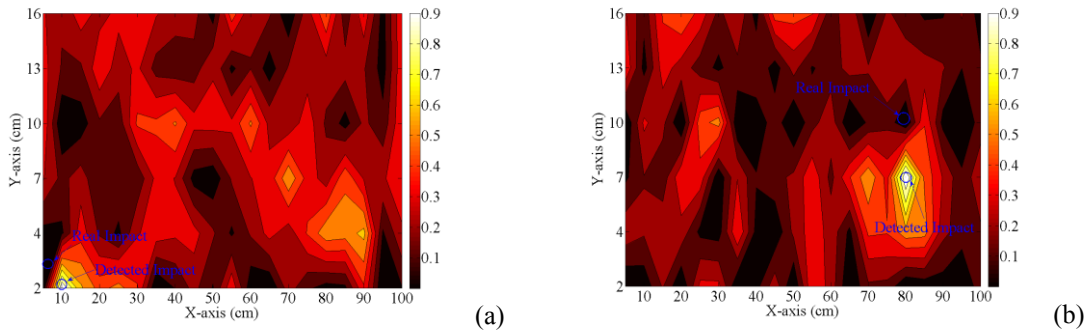

Figure 8 2D map of the impact Br1 with M = 13 x 5 excitation points (a) and Br2 with M = 10 x 4 excitation points (b) using IF on the composite blade.

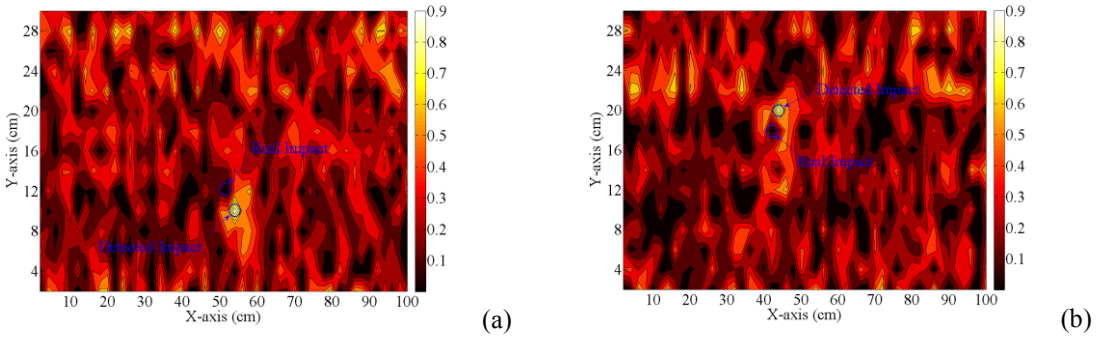

Figure 9 2D map of the impact Sr1 with M = 40 x 12 excitation points (a) and Sr2 with M = 37 x 11 excitation points (b) using IF on the stiffened panel.

The excitation points were randomly chosen over the surface of the structures and all the impacts were applied in points that were not included in the library of signals acquired in the "forward propagation step". However, the imaging results illustrated in Figs. 8 and 9 showed that the highest correlation coefficient associated to the detected focusing source corresponds to the cell nearest to the real impact location. The error estimation in retrieving the impact location was provided by the impact localisation error χ that is given by the formula $\chi = \sqrt{(x_m - x_{m0})^2 + (y_m - y_{m0})^2}$, where x_m and y_m and x_{m0} and y_{m0} are the coordinates of the detected and real impact point, respectively. Notably, for all the impact tests on both the composite blade and the stiffened panel, the localisation error χ was found of the order of the single cell size on the "focusing plane". This information not only strengthens the effectiveness of the IF process to focus the wave energy at the impact point in space and time, but also it might open to scenarios in which a limited sparse set of excitation sources can be used to back propagate diffuse wave fields at the impact location.

IV.3 Imaging Results with Reduced Receiver Sensors

According to Section II.2, although one single receiver transducer is needed to perform the IF imaging process, a weighted average from the contribution of L surface bonded receiver sensors allows compensating the incoherent measurement noise due to electronics (sensor noise, electronic noise, etc…). Table 7 shows the impact localisation results on both structures for a number of experiments with different receiver sensors configurations. Particularly two impact tests with their associated in-plane coordinates are reported for each composite structure. The "O" letter corresponds to a perfect matching between the detected coordinates through the IF imaging process and the real ones.

	Tail Rotor Blade (real coordinates)				**Stiffened Panel (real coordinates)**			
L	**X (cm) 5**	**Y (cm) 1**	**X (cm) 16**	**Y(cm) 3**	**X (cm) 1**	**Y (cm) 13**	**X (cm) 10**	**Y (cm) 3**
1,2,3,4	O	O	O	O	O	O	O	O
2,3,4	4	2	O	O	2	O	O	O
1,3,4	O	O	O	2	O	14	O	O
1,2,4	O	O	O	2	O	O	11	O
1,2,3	O	2	O	2	2	O	O	2
3,4	6	2	O	2	O	11	O	O
2,4	O	O	O	2	2	O	O	2
2,3	6	O	17	O	O	14	9	O
1,4	O	O	15	2	O	14	11	O
1,3	O	O	15	O	2	O	11	O
1,2	4	2	O	O	O	O	11	O
1	4	2	O	O	2	12	O	O
2	4	O	O	O			O	2
3	6	3	15	2	O	12	O	O
4	6	3	15	2	O	14	O	4

Table 7. Imaging results using different combinations of receiver sensors. The "O" letter corresponds to an exact value of the coordinate.

The experimental results reported in Table 7 were carried out with the original number of excitation points according to Section IV.1 and the results showed that the sensitivity of the re-focusing process with reciprocal TR was enhanced by adding sensors up to L = 4 (as already noticed through the paper). This was the only case in which no errors on

the impact location were found. Indeed, the more the number of receiver sensors decreases, the highest is the possibility of a wrong estimation of the impact location. However, it still can be seen that for those receivers' combinations in which the real focus point was different from the detected one, the localisation error χ was relatively low (of the order of the cell size).

V. Conclusions

This paper analysed the factors affecting the impact localisation refocusing approach using a reciprocal time reversal method. Particularly, a simple signal stretch procedure known as "forward step signal stretch" (FSSS) was developed to compensate the temperature changes of diffuse wave fields that led to either a dilatation or contraction of the acoustic waveforms measured by a finite number of receivers transducers. Then, in order to decrease the computational demand of the stored signals but not the sensitivity of the inverse filtering process, different set of libraries with reduced excitation point were investigated. The experimental results on both a composite tail rotor blade and a stiffened panel undergone to impact loadings showed the effectiveness of the FSSS coupled to reciprocal time reversal for a number of impact events. Moreover, IF process demonstrated high accuracy in focusing the acoustic energy at the impact point both in space and time, even reducing the number of excitation points. Finally, although one single receiver sensor is theoretically required to perform the reciprocal time reversal process, this research work experimentally showed that the presence of incoherent measurement noise due to electronics could generate imaging ambiguities in retrieving the impact location. This further negative effect could be

eliminated by using the weighted contribution of additional receiver sensors on both structures.

References

Atobe S, Fukunaga H, Hu N (2011) Impact force identification of CFRP structures using experimental transfer matrices, *Computers Materials & Continua*, **26**(1), 67-90.

Atobe S, Sugimoto S, Hu N, Fukunaga H (2014) Impact damage monitoring of FRP pressure vessels based on impact force identification, *Advanced Composite Materials*, **23**, 491-505.

Caputi WJ, (1971) Stretch: A time transformation technique. IEEE Trans. Aerospace Electron. Syst., vol. AES-7, pp.269 -278.

Catheline S, Queffin N, Ing RK, Fink M (2007) Acoustic source localization model using in-skull reverberation and time reversal. *Appl. Phys. Lett.* **90**, 063902.

Ciampa F, Meo M (2010a) Acoustic emission source localization and velocity determination of the fundamentl mode A_0 using wavelet analysis and Newton-based optimization technique", *Smart Mater. Struct.* ***19,*** 1-14.

Ciampa F, Meo M (2010b) A new algorithm for acoustic emission localization and flexural group velocity determination in anisotropic structures. *Compos. Part A* **41**:1777-1786.

Ciampa F, Meo M (2011) Acoustic emission localization in complex dissipative anisotropic structures using a one-channel reciprocal time reversal method. *J. Acoust. Soc. Am.* **130** (1), 168-175.

Ciampa F, Meo M (2012a) Impact detection in anisotropic materials using a time reversal approach. *Structural Health Monitoring* **11** (1), 43-49.

Ciampa F, Meo M (2012b) Nonlinear elastic imaging using reciprocal time reversal and third order symmetry analysis. *J. Acoust. Soc. Am.* **131**, pp. 4316–4323.

Clarke T, Simonetti F and Cawley P (2010) Guided wave health monitoring of complex structures by sparse array systems: Influence of temperature changes on performance. *J. Sound Vib.* **329** 2306–22.

De Marchi L, Marzani A, Speciale N, Viola E (2011) A passive monitoring technique based on dispersion compensation to locate impacts in plate-like structures. *Smart Mater. Struct.* ***20,*** 035021.

Ciampa F, Meo M (2014) Impact localization on a composite tail rotor blade using an inverse filtering approach. *Journal of Intelligent Material Systems and Structures,* ***25*** *(15), pp. 1950-1958.*

Hu N, Fukunaga H, Matsumoto S, Yan B, Peng X.H (2007) An Efficient Approach for Identifying Impact Force Using Embedded Piezoelectric Sensors, *International Journal of Impact Engineering*, **34**, 1258-1271.

Ing RK, Quieffin N, Catheline S, Fink M (2005) In solid localization of finger impacts using acoustic time-reversal process. *Appl. Phys. Lett.* **87**, 204104.

Landau LD, Lifshitz EM (1960) Theory of elasticity", (2nd English ed.) Pergamon, New York.

Larose E, Margerin L, Derode A, van Tiggelen B, Campillo M, Shapiro N, Paul A, Stehly L, Tanter M (2006) Correlation of random wavefields: An interdisciplinary review. *Geophysics* **71**, SI11-SI21.

Leroy V, Derode A (2008) Temperature-dependent diffusing acoustic wave spectroscopy with resonant scatterers. *Phys. Rev. E* **77**, 036602.

L di Scalea F, Salamone S (2008) Temperature effects in ultrasonic Lamb wave structural health monitoring systems. *J. Acoust. Soc. Am.* ***124*** (1), 161-174.

Lobkis OI, Weaver R (2001) On the emergence of the Green's function in the correlations of a diffuse field. *J. Acoust. Soc. Am.* **110** (6), 3011–17.

Lu Y, Michaels JE (2005) A methodology for structural health monitoring with diffuse ultrasonic waves in the presence of temperature variations. *Ultrasonics*, **43** (9) 717–731.

Ribay G, Catheline S, Clorennec D, Ing RK, Quieffin N, Fink M (2007) Acoustic impact localization in plates: properties and stability to temperature variation. *IEEE Trans. Ultrason. Ferroelectr. Freq. Control* **54**, pp. 378–385.

Snieder R, Gret A, Douma H, Scales J (2002) Coda wave interferometry for estimating nonlinear behavior in seismic velocity. *Science* **295** (5563) 2253–2255.

Tanter M, Thomas JL, Fink M (1998) Focusing and steering through absorbing and aberrating layers: Application to ultrasonic propagation through the skull. *J. Acoust. Soc. Am.* **103** (5), 2403–10.

Ulrich TJ, Van Den Abeele K, Le Bas PY, Griffa M, Anderson BE, and Guyer RA (2009) Three component time reversal: Focusing vector components using a scalar source. *J. Appl. Phys.* **106**, 113504.

Van Damme B, Van Den Abeele K, Li Y, Matar OB (2011) Time reversed acoustics techniques for elastic imaging in reverberant and nonreverberant media: An experimental study of the chaotic cavity transducer concept. *J. Appl. Phys.* **109** (10), 104910.

Weaver R (1982) On diffuse waves in solid media. J. Acoust. Soc. Am. 71 (6), 1608–09.

Weaver RL, Lobkis OI (2000) Temperature dependence of diffuse field phase. *Ultrasonics* **38** 491–494.

Worden K, Farrar CR, Manson G, Park G (2007) The fundamental axioms of structural health monitoring. *Proceedings of the Royal Society A,* **463,** 1639–1664.